Assessment of a Hybrid-Based Approach with a Random Forest Ensemble for Determination of Shallow Water Depths from Multispectral Satellite Images

Mohamed, H.[1]* and Nadaoka, K.[2]
[1]Department of Geomatics Engineering, Shoubra Faculty of Engineering, Benha University, Cairo, Egypt, E-mail: hassan.mohamed@ejust.edu.eg, hassan.hussein@feng.bu.edu.eg
[2]Department of Transdisciplinary Science and Engineering, School of Environment and Society, Tokyo Institute of Technology, Tokyo, Japan, E-mail: nadaoka.k.aa@m.titech.ac.jp
Corresponding author

Abstract
In this study, an approach is proposed for determining the depths of shallow waters from multispectral satellite images. This approach is a hybrid system that uses a Random Forest Ensemble (RFE) technique for Neural Network (NN) and Support Vector Regression (SVR) algorithms to improve accuracy of bathymetry estimations by reducing both errors and prediction variance. The study was performed over two different coastal areas: the first is the port of Alexandria, Egypt, which has a low turbidity silt–sand bottom area with a depth range of 10.5 m; the second area is Shiraho, Japan, which is a heterogeneous bottom composition coral reef area with a varied depths range up to 12.5 m. Landsat-8 and Quickbird satellite images were used for these two study areas, respectively, as examples of low- and high-resolution images. These images were corrected for both atmospheric and sun-glint errors. The results were validated using echosounder field points. Four reflectance values of green, red, blue divided by red, and green divided by red bands were assigned to reference point locations. These values were used for algorithm training and testing processes. The SVR and NN output values were combined using RFE. In order to evaluate the accuracy of the BE approach, we compared its outputs to that of the NN and SVR approaches. All of the results were evaluated using RMSE and R^2 values. The RFE approach was found to yield a RMSE of 0.64 and 0.90 m for the two areas, resulting in an almost 20 and 10 cm improvement. These results suggest that the proposed RFE approach outperforms both the NN and SVR algorithms, when they are used individually.

1. Introduction

Coastal area bathymetry plays an important role in a wide variety of fields and applications, such as coastal engineering, coastal oceanography, spatial monitoring, and sustainable management of coastal and lake areas (Leu and Chang, 2005 and Gao, 2009). Sediment movement in shallow coastal areas occurs due to tidal currents, waves, nearshore currents, and intensive human activities (Ceyhun and Yalçın, 2010). Therefore, accurate and regularly updated methods, mainly focusing on measuring the water depths, for such areas should be developed (Pacheco et al., 2015).

Currently, single and multibeam echosounders and Light Detection and Ranging (LiDAR) are the most widely used methods for bathymetric applications. Although these methods are highly accurate at detecting depths, they are costly and difficult to use, especially, in shallow areas where coral reefs, rocks, and shallowness act as obstacles to the navigation of survey vessels (Chust et al., 2010). Recently, airborne LiDAR technology has been developed and has been used in bathymetric applications (Su et al., 2008). Nevertheless, the LiDAR technology is not only expensive and time consuming but also requires exhaustive labor than the traditional single and multibeam echosounders. Optical satellite images are a low-cost, wide-coverage, and time-effective alternative to the traditional methods used for bathymetric applications (Sánchez-Carnero et al., 2014). A variety of optical satellites with more developed spatial and radiometric resolutions were recently launched and used to estimate water depths; some of these satellites include Landsat (Fuxing, and Qian, 2003), (Hoepffner and Zibordi, 2009), SPOT (Kao et al., 2009 and Sánchez-Carnero et al., 2014), IKONOS (Stumpf et al., 2003 and Paringit and Nadaoka, 2012), WorldView-2 (Doxani et al., 2012 and Kibele and Shears, 2016), and RapidEye (Monteys et al., 2015).

A literature review revealed that a number of different approaches have used satellite images to perform bathymetry. One type of approach involves analytical methods that use look-up tables or spectral libraries (Louchard et al., 2003, Lesser and Mobley, 2007, Brando et al., 2009 and Jay and Guillaume, 2014). These analytical approaches requires a hyperspectral images for processing. As these images can provide sufficient information about the reflectance from a submerged surface as well as suspended and dissolved matters (Vahtmäe and Kutser, 2016). However, these particular approaches have a number of drawbacks; for example, hyperspectral images are not available over large areas and have coarse spatial resolutions. Moreover, these images require extensive processing times and relatively complex processing methods. Alternative empirical methods include the linear band model (Lyzenga, 1985), the wave kinematics bathymetry method (Piotrowski and Dugan, 2002), the bands ratio transform model (Stumpf et al., 2003), the least-squares fit model (Lee et al., 2011), and the k-nearest neighbor model (Kibele and Shears, 2016). However, most of these empirical algorithms assume that the water column is similar and the environmental factors are homogenous over the entire area being observed (Su et al., 2008). This assumption may decrease the accuracy of depth measurements as these factors are not found in most areas. In addition, linear techniques, such as the Lyzenga model (Lyzenga et al., 2006) and the least-squares fit regression model, result in poor bathymetry measurements due to the bathymetric system's nonlinear nature (Paul and Roehl, 2006).

Ceyhun and Yalçın (2010) recently proposed an alternative approach for detecting water depth; their technique utilized an artificial neural network (NN). NNs are flexible mathematical structure models that are capable of performing nonlinear functions between the spectral bands of satellite images and water depth values. As a result, they are able to overcome the limitations of the abovementioned regressive models discussed earlier in this section. Numerous studies have used NN algorithms to determine water depths from satellite imagery. For example, NN approaches were combined with Landsat images (Gholamalifard et al., 2013), IRS P6-LISS III (Moses et al., 2013), and Quickbird images (Corucci et al., 2011). These particular studies found that the NNs outperformed other empirical methods. In addition, random forest ensemble regression trees can be used for highly accurate bathymetry mapping; this approach is less affected by environmental factors than other empirical methods and it is invincible to overfitting drawback as compared to NN method (Mohamed et al., 2017). The present study proposes a hybrid approach that uses RFE for bathymetry purposes in shallow coastal areas. The proposed algorithm offers complementary information from both the NN and SVR approaches and, as a result, the obtained depths can be improved. The RFE methodology was then tested using free Landsat-8 and Quickbird images. Finally, the obtained bathymetry results were evaluated by an echosounder field measurement performed over two different areas.

2. Study Areas and Available Data

2.1 Study Areas

Two different areas to be studied were selected. The first study area was Alexandria harbor, Egypt (see Figure 1).

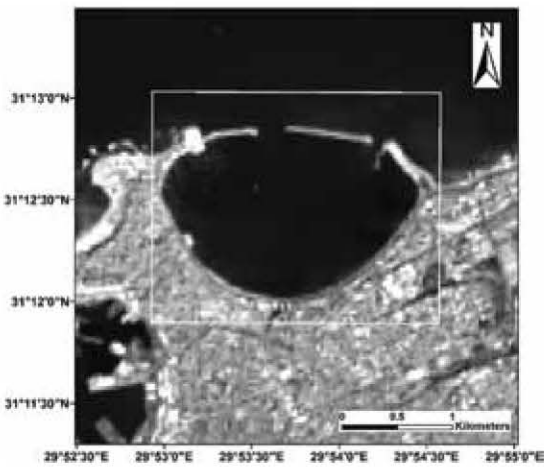

Figure 1: The 1st study area of Alexandria port coastal area, Egyp

Figure 2: The 2nd study area of Shiraho, Ishigaki Island, Japan

It is a deep and calm water area with low turbidity and has a depth range of 10.5 m. Most of the port seabed area is covered with silt and sand. The second area of study was Shiraho, a sub-tropical region that is located in the south-eastern part of Ishigaki Island, Japan (see Figure 2). It is a shallow water area with non-uniform bottom composition, and the depth range is up to 12.5 m. Shiraho is an area of rich marine biodiversity, and there are numerous ecosystems, such as algae, sediments, seagrass, and coral reefs.

2.2 Imagery Data

Freely available Landsat-8 and Quickbird satellite images were used for the bathymetry measurements of the first and second study areas, respectively. The Landsat-8 images had a spatial resolution of 30 m, and they were captured during calm weather conditions on 22 March 2014. Moreover, the Quickbird images had a spatial resolution of 0.6 m and were collected during windy conditions on 20 July 2007. The Landsat-8 images were selected so that they could be synchronized with the echosounder field measurements time for the port of Alexandria area. The sounding field data for the Shiraho area was collected on 25–31 January 2013. Note that for Shiraho area there was a time difference between when the images were taken and when the field data was taken. As Shiraho area did not experience any tsunamis or abnormally large waves during these years, the time difference was not expected to have a significant impact on the bathymetry measurements (Collin et al., 2014). The required values for imageries processing or radiometric calibrations were presented in the images' metadata files.

2.3 Echo-Sounder-Benthic Cover Field Data

The depth of the water in the first study area was measured by a NaviSound Hydrographic Systems model 210 echosounder device that had a Trimble 2000 GNSS instrument attached to it. This echosounder system is able to make measurements to depths of 400 m, and its vertical accuracy is 1 cm at 210 kHz (see Figure 3). In addition, measurements of the depth of the water of the second study area were collected by a single-beam Lowrance LCX-15MT dual frequency (50/200 kHz) transducer with a 12-channel GNSS antenna (see Figure 4). The horizontal and vertical accuracies of the Lowrance device were ±1 m and ±0.03 m, respectively (Heyman et al., 2007). Approximately 2500 and 8106 field points were measured in the first and second study areas, respectively, and they were referenced to that of the mean sea level. These field points were used to calibrate and evaluate all of the bathymetric approaches investigated in this study.

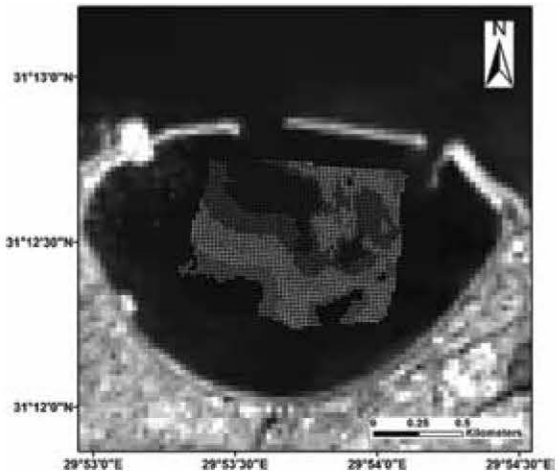

Figure 3: Field bathymetry observed points of 1st study area from echo-sounder

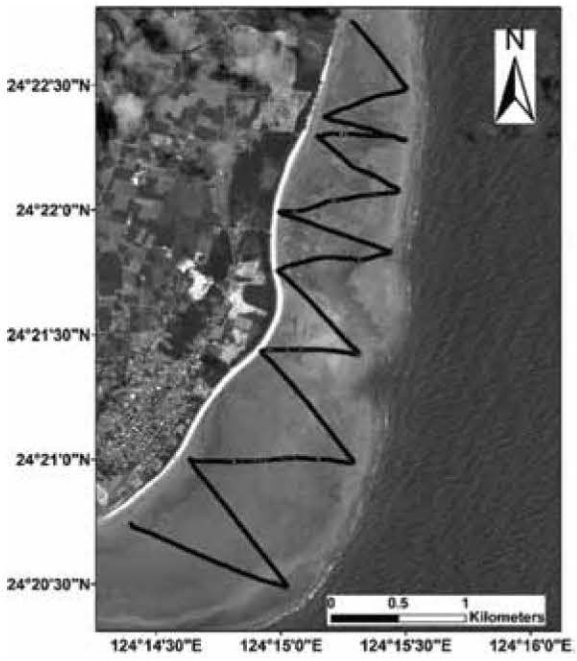

Figure 4: In-situ bathymetry observed points of 2nd study area from echo-sounder

3. Methodology

Both the Landsat-8 and Quickbird multispectral images were preprocessed for bathymetric mapping by the following steps: first, the image pixel values were converted to radiance values through the use of the metadata file values of the images. Atmospheric corrections were then performed on the image radiance values with the FLAASH tool. The input parameters for the FLAASH tool were defined as

illustrated in the methodology sec 3.1.2. The resultant images from the atmospheric correction were checked against the field signal curves for each reflectance value. Lastly, the atmospherically corrected values were subject to sun-glint corrections that were made using the Hedley method (Hedley et al., 2005). All of the abovementioned steps were performed in an ENVI 5.3 environment.

For the bathymetry mapping, both the NN and SVR approaches were applied to the preprocessed Landsat-8 and Quickbird multispectral images, and their predicted outputs were combined using the RFE algorithm. The input values for the NN and SVR approaches were extracted from the corrected images at the corresponding locations of the echosounder reference points. Four inputs that were extracted from the corrected reflectance images were used for training all the approaches at the same locations of the field sounding points. These input values were red, green, blue divided by red, and green divided by red bands logarithms then the outputs were the predicted water depths.

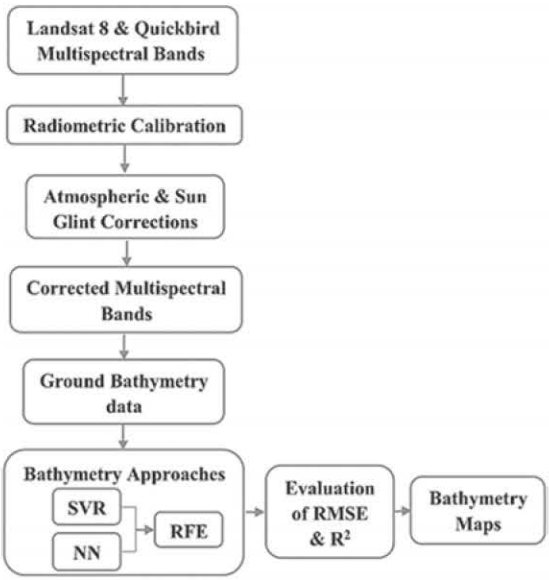

Figure 5: Processing steps for bathymetry detection using BE approach

For all of the study areas, these values were randomly separated, with 65% of the values being allocated to training, 10% to validation, and 25% to testing. For example, the Shiraho study area field points were divided into 5472, 608, and 2026 points for training, validation, and testing, respectively. The RFE approach was then applied to ensemble the outputs from the NN and SVR methods. The validation points were used to train the RFE approach, with the NN and SVR outputs being used as input values and the predicted water depth values as outputs. Finally, all of the outputs from the various approaches were evaluated using the same independent testing points, depending on the RMSE and R^2 values (see Figure 5).

The SVR kernel function was fine Gaussian with 0.5 kernel scale. On the other hand, the NN training function was the Levenberg–Marquardt backpropagation with 10 hidden layers, while the RFE algorithm ensemble the output values from SVR and NN approaches with 50 trees and a two thirds split percentage. These parameters were selected for each algorithm based on the least possible RMSE and highest R^2 values. All of these algorithms were implemented in a Matlab environment.

3.1.1 Spectral top of atmosphere radiance

The Landsat-8 and Quickbird data were provided as digital number (DN) images. These DN values were converted to spectral top-of-atmosphere radiance values for each pixel; these values denote the amount of energy received by the sensor. This conversion can be applied through the use of the following equation (Landsat-8, 2013):

$$L\lambda = G * DN + I \quad \text{Equation 1}$$

Where $L\lambda$ = top-of-atmosphere spectral radiance, DN = digital number recorded by the sensor, G = band-specific multiplicative rescaling factor for radiance values, and I = band-specific additive rescaling factor for radiance values. Both the G and I values can be found in the metadata files of the images.

3.1.2 Atmospheric correction

Both the Landsat-8 and Quickbird images were corrected for atmospheric errors using the fast line-of-sight atmospheric analysis of hypercubes (FLAASH™) algorithm in the Envi 5.3 program. Numerous studies have used the FLAASH algorithm to perform atmospheric corrections, especially, when conducting bathymetry measurements (Blakey et al., 2015, Lyons et al., 2011 and Wahidin et al., 2015). The radiance values calculated as part of 2.4.1 were used as inputs for the FLAASH algorithm. FLAASH performs a radiative transfer model on the obtained data by using a MODTRAN4 code (Berk et al., 1998) beside using look-up tables for diverse categories of atmosphere (Liu and Zhou, 2011). Moreover, the FLAASH algorithm contains various types of aerosols that define the properties of the particles in the atmosphere. For our two study areas, we chose

the maritime type for the aerosol model, the tropical type as the atmospheric model, and the blue and near-infrared bands as the aerosol retrieval type over water areas (Su et al., 2008). This step finally produced atmospherically corrected reflectance images.

3.1.3 Sun glint correction

A literature review revealed that there are various methods for correcting sun glint (Kay et al., 2009). The Hedley method is the most widely used method for correcting sun glint (Hedley et al., 2005). This method uses the relationship between the bands used for bathymetry mapping and the near-infrared band because the near-infrared band has a negligible amount of sun glint (Hedley et al., 2005 and Sánchez-Carnero et al., 2014). The atmospherically corrected reflectance images had sun-glint corrections applied to them. Moreover, the corrected pixel values can be calculated using a sample of pixels and the following equation:

$$Li\ (VIS)' = Li\ (VIS) * bi\ (LNIR - Lmin\ (NIR)) \quad \text{Equation 2}$$

Where Li (VIS)' = de-glinted pixel reflectance values, Li (VIS) = atmospherically corrected reflectance values, bi = regression line slope, LNIR = corresponding pixel values in the near-infrared band, and Lmin (NIR) = minimum near-infrared values existing in the sample.

3.2 Proposed Algorithms for Bathymetry Mapping

3.2.1 Support vector regression

Vapnik and Chervonenkis (1964) offered support vector machines (SVMs) for classification applications and solving statistical problems. Support Vector Regression (SVR) targets to nd a linear hyperplane, which can ts the multi-dimensional input vectors to output values. At that point, the outcome can be used to predict future output values that are contained in a separated testing set. As instance, in any regression problem, suppose that we have a training dataset of $D = (y_i, t_i$ and $i = 1, 2, 3 \ldots n)$ with input vectors y_i and target vectors t_i. So, the main regression algorithm target is to find a fitting function f (y) that estimates the relationship between the input and target points (Mohamed et al., 2017). For linear functions f, the hyperplane that is constructed by the SVR is determined as follows:

$$f(x) = w * y + b \quad \text{Equation 3}$$

The predicted value, f (x), depends on a slope (w) and an intercept (b) which displays relationships to a linear regression model.

Flatness in the regression problems can be solved by minimizing the norm Euclidian space $|w|^2$. As a result, the problem of nding an optimum hyperplane is a convex optimization problem. Moreover, to solve the non-linear relations between input vectors and outputs it is necessary to define a map (ϕ) that transforms the training points x into a higher-dimensional feature space. The result is that w, after creating a Lagrangean function from Equation (1) will be a function of $\phi\ (x_i)$ and that the product $\phi\ (x_i)\ \phi\ (x)$ needs to be calculated (Smola and Schölkopf, 2004). This function $\phi\ (x_i)\ \phi\ (x)$ is identified as a kernel function K (xi, x). In other words, SVMs use kernel functions to project the data on a new hyperspace to simply represent the complex non-linear patterns (Williams, 2011 and Were et al., 2015).

3.2.2 Neural network

The supervised multilayer perception (MLP) approach combined with the back propagation (BP) method can be used as a training algorithm to determine the nonlinear relationship between input and output data (Rumelhart et al., 1986). This approach comprises three parts: the input layers act as neurons, which are the multispectral image band values in bathymetry detection problems; the hidden layer is used to control the network training procedure; and the output layer describes the predicted water depth (Gholamalifard et al., 2013). The BP algorithm attempts to reach a predefined level of accuracy. As a result, the algorithm starts with initial weightings that are used to find values with the highest levels of accuracy; it does this by comparing predicted outputs with desired values in an iterative process (Razavi, 2014). As it is the most widely used algorithm in the training process of MLP approaches, the Levenberg–Marquard training algorithm was used in the BP training process in this study (Ranganathan, 2004). Finally, a log-sigmoid function was selected for the transferring of the neural network input values to the final node output values. Since the derivative of the log-sigmoid function can be easily computed and it is widely used already (Ceyhun and Yalçın, 2010).

3.2.3 Random forest

The random forest (RF) is an ensemble of decision trees that have been created from learning sample groups that have been assembled independently from a training sample (Breiman, 2001). The training of the RF algorithm is achieved through the use of a bootstrap aggregating technique.

In this technique, numerous trees are created, and each tree is trained on a bootstrapped sample of the training data with replacement. Bootstrapped sampling means that the selected data for decision trees training process is not eliminated from the next generated subset of data. In addition, the RF method was improved such that for each tree splitting at every single node, the best split among a subset of predictors randomly chosen were used (Kim and Sohn, 2011). The random feature selection improves both the overall accuracy of the method as well and the variation between sample trees, and it prevents overfitting. The final prediction will be calculated using averaging or majority voting techniques for regression or classification problems, respectively (Ghimire et al., 2012). Two predefined parameters are required before RF can be used: the amount of samples used to split each node and the number of developed trees (Guan et al., 2012). The remaining amount of calibration variables, known as out-of-bag data, can be used to estimate the regression accuracy. For regression problems, setting the splitting percentage to be two thirds of the overall data usually achieves the most accurate results (Breiman, 2014). An impurity criterion or attribute selection measurement must then be applied so that the best split selection at each node is made. One of the most widely used example of such criterion is the Gini diversity index (Immitzer et al., 2012).

4. Results

Figures 6-8 shows the bathymetric maps that were computed by applying each model to the Landsat-8 and Quickbird satellite images for each study area, while Figures 7-9 show the evaluation of each model; Tables 1-3 summarize the corresponding RMSE and R^2 values. Meanwhile, Tables 2-4, present the RMSE values for various depth ranges for each method over the two study areas.

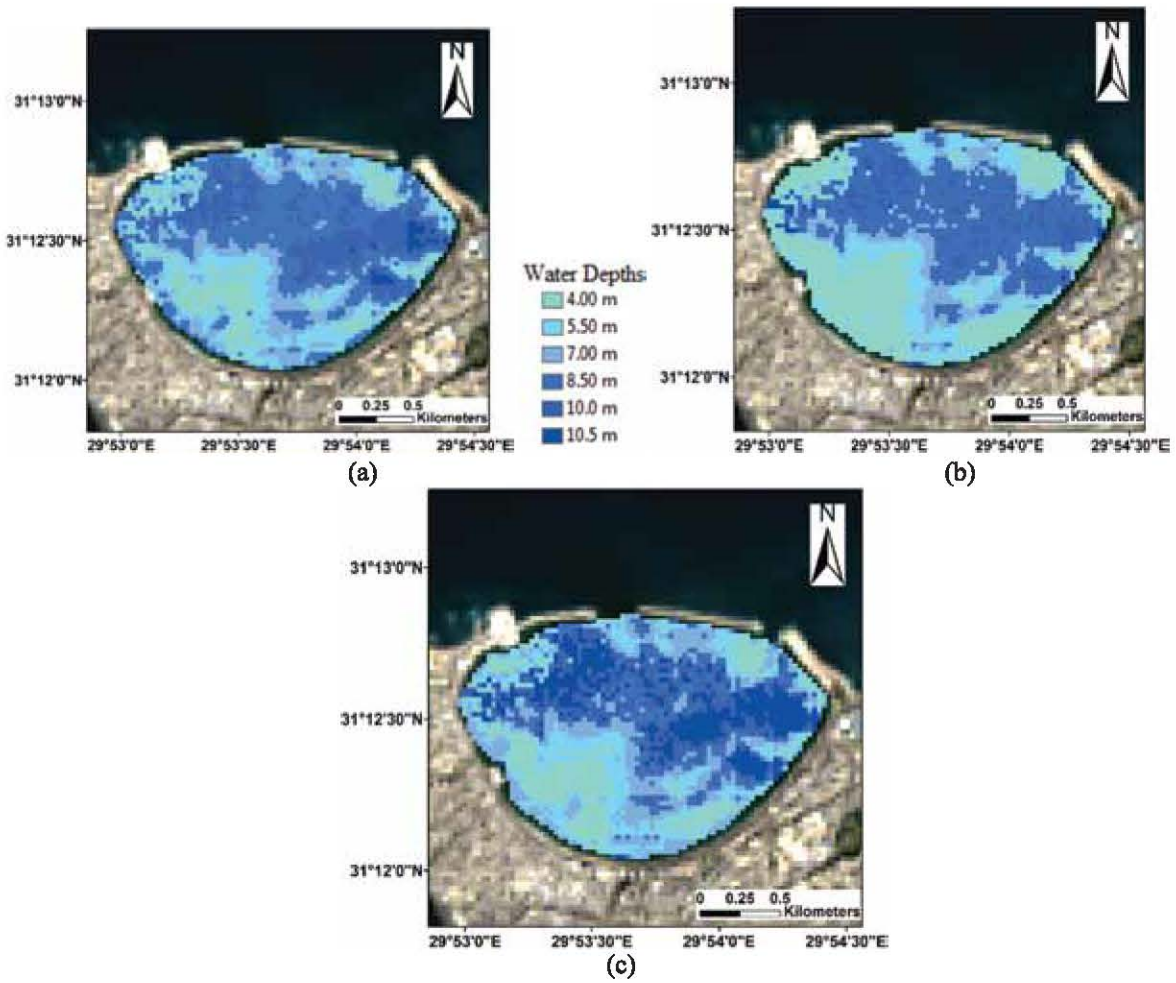

Figure 6: Bathymetric maps derived by applying each algorithm using Landsat-8 imagery over Alexandria harbor area, Egypt. (a) SVR (b) NN (c) RFE

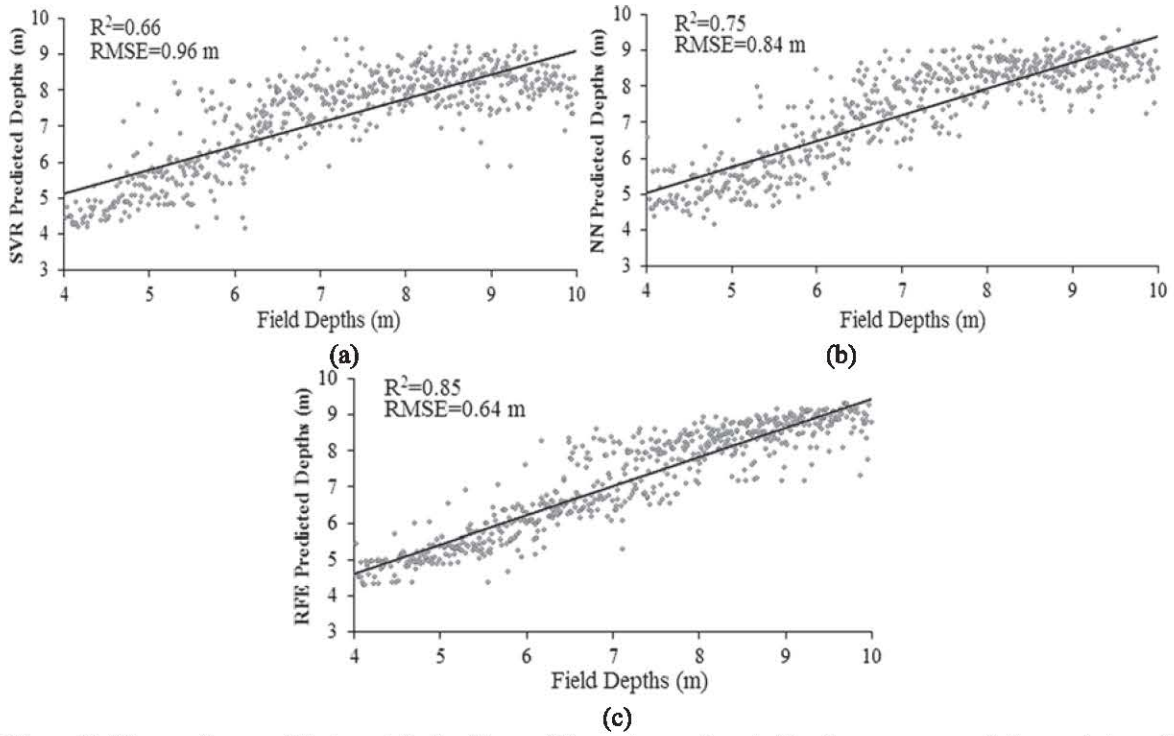

Figure 7: The continuous fitted models for Alexandria port area, Egypt. Depths are represented as points, and the continuous line represents the continuous fitted model (a) SVR (b) NN (c) RFE

Table 1: The RMSEs and R^2 of all methods for bathymetry detection over Alexandria port area, Egypt

Methodology	SVR	NN	RFE
RMSE (m)	0.96	0.84	0.64
R^2	0.66	0.75	0.85

Table 2: The RMSEs (in meters) of all bathymetry detection methods in three levels of depths for Alexandria port area, Egypt

Methodology	SVR	NN	RFE
4-6 m	0.86	0.80	0.56
6-8 m	0.90	0.87	0.66
8-10.5 m	1.09	0.85	0.68

Table 3: The RMSEs and R^2 of all methods for bathymetry detection for Shiraho Island, Japan

Methodology	SVR	NN	RFE
RMSE (m)	1.03	0.98	0.90
R^2	0.834	0.851	0.872

Table 4: The RMSEs (in meters) of all bathymetry detection methods in three levels of depths for Shiraho Island, Japan

Methodology	SVR	NN	RFE
0-4 m	0.84	0.81	0.75
4-8 m	1.25	1.16	1.08
8-12.5 m	1.53	1.43	1.32

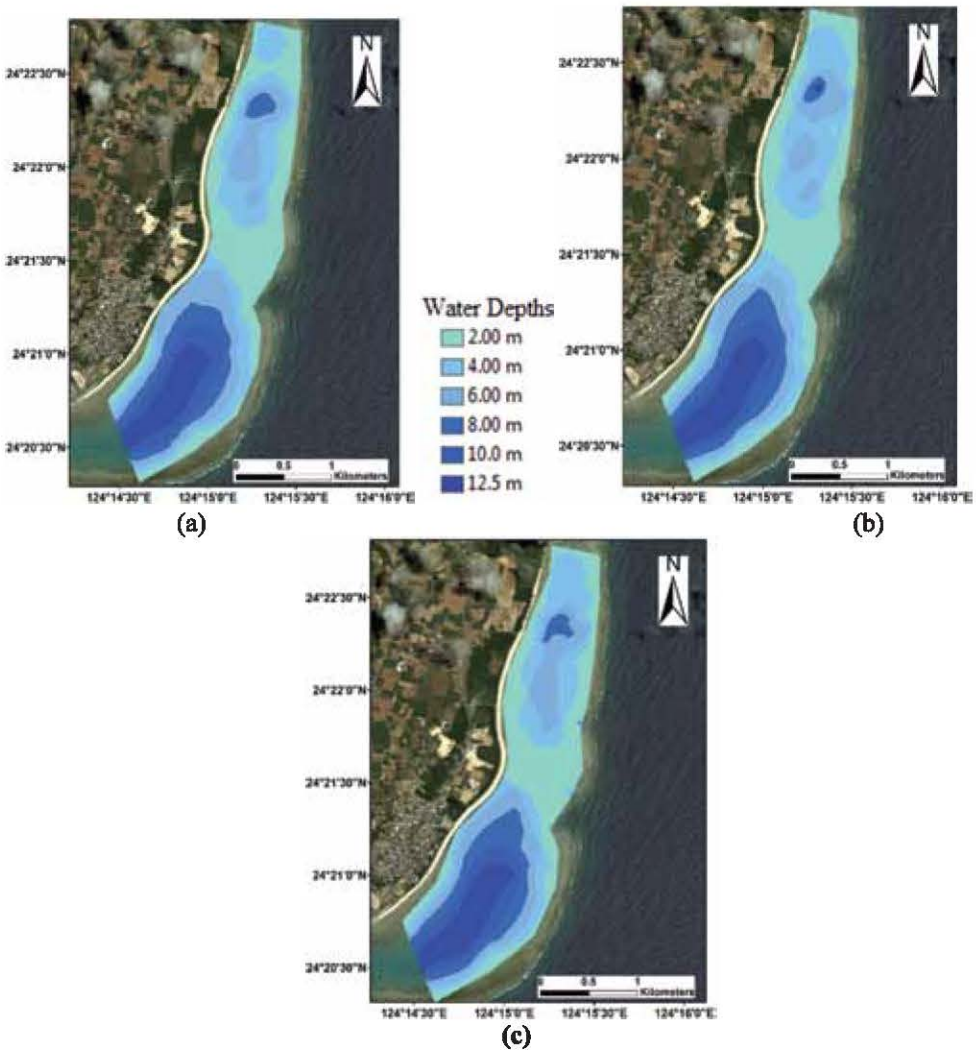

Figure 8: Bathymetric maps derived by applying each algorithm using Quickbird imagery over Shiraho Island area, Japan. (a) SVR (b) NN (c) RFE

5. Discussion

Appropriate bands for the bathymetry estimations were selected through a statistical analysis, which was used to investigate the correlation between the water depth values obtained and the satellite imagery bands. This investigation confirmed that there was a robust correlation between the red and green bands and the water depth values (Su et al., 2008 and Stumpf et al., 2003). However, the blue bands in the Landsat-8 and Quickbird images showed a slight correlation with the water depth values in the two coastal areas. This slight correlation can be explained by the absorption of coastal and blue bands signals by the dissolved organic matters and phytoplankton in the water column (Gholamalifard et al., 2013).

The SVR algorithm is a stable approach that uses the optimum kernel function to correlate the imagery bands with water depth. This correlation can be performed by creating an optimum hyperplane that ts data and predicts with the minimum complexity of the modelling function. In this study, the optimum kernel function was selected, after several trials, based on minimum RMSE and maximum R^2. In this study, the optimum kernel function was fine Gaussian with 0.5 kernel scale. Alternatively, the NN approach formed a correlation between the imagery bands as inputs and water depth values as predicted outputs using multidimensional nonlinear functions. Previous studies (Ceyhun and Yalçın, 2010 and Gholamalifard et al., 2013) have proved the superiority of NN approaches over those of classical empirical models such as Stumpf et al., (2003) or Lyzenga et al., (2006). However, NN approaches suffer from significant drawbacks.

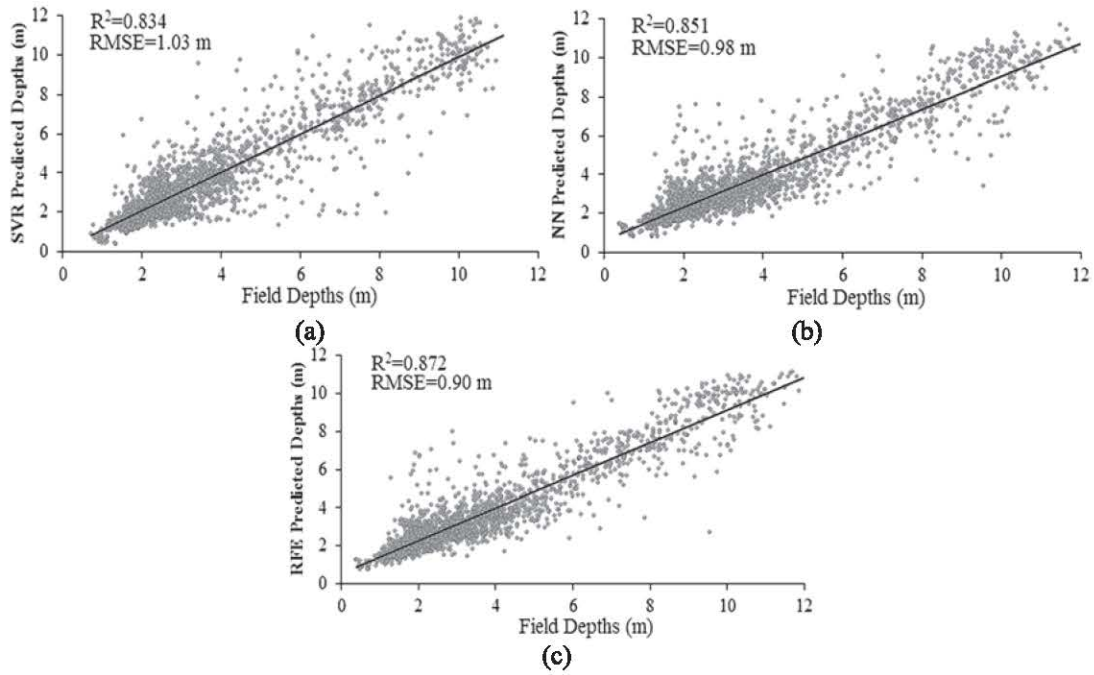

Figure 9: The continuous fitted models for Shiraho Island, Japan. Depths are represented as points, and the continuous line represents the continuous fitted model (a) SVR (b) NN (c) RFE

For example, they require a lot of attempts before they can determine the best weights of correlation. As NN is an unstable technique that results in different RMSE and R^2 values from one trail to another.

RFE is a fitting ensemble of a regression trees method that averages the regression trees generated by a bootstrapped selection from an input sample. The optimal number of regression trees was selected after successive trails with numerous numbers of trees (10, 20, 30... 100), and the best RMSE and R^2 values were obtained with 50 trees. The Gini index criterion was also used for the trees splitting. The creation of random regression trees and the splitting of the data into training and testing sets confirmed that the RFE approach was not overfitting the input data. In order to demonstrate the precedence of the proposed RFE algorithm, it was tested over two different areas with various water column characteristics and bottom coverage. Particularly, Shiraho area which has a heterogeneous bottom cover and variations in the water optical properties. Figures 7 and 9 shows a scatter plot of the predicted depths versus the field depths, obviously, there is a variation of the results within each of these depth intervals. As we removed the atmospheric errors so the remained errors result from variations in either the water optical properties or the bottom composition. However, the proposed RFE approach increased the resulted accuracy compared to NN or RF approaches.

The RFE approach was applied so as to ensemble the outputs from the NN and SVR methods. The main advantage of enacting such a combination is that it allows us to exploit the differences between the two approaches, and combining these approaches increases the overall accuracy of the NN and SVR methods because they have different sources of errors and weaknesses. The obtained results in this study confirmed that this combination increased the depths determination accuracy by approximately 20 and 10 cm over a silt–sand and coral reef areas, respectively. An additional merit of the proposed approach is its ability to produce accurate results even with a limited number of training samples.

In order to compare our results with those of comparable studies, many factors have to be considered. These factors include the spatial resolution of the images, the bottom-type, water turbidity, availability of an adequate number of field points in a study area, and the depth range. For example, Vinayaraj et al., (2016) argued that the adaptive geographically weighted regression (A-GWR) model is the most suitable model for bathymetry estimations in clear waters in heterogeneous coastal areas. The A-GWR model yielded a RMSE of 1.14 and 0.40 m for the Landsat-8 and RapidEye images, respectively, at a depth range of 20 m. Pacheco et al., (2015) tested Landsat-8 coastal, blue, and green bands for bathymetry estimations using the Lyzenga linear model over

clear waters in a shallow coastal area and they obtained a RMSE of 1.01 m at a depths range of 12 m. Kibele and Shears, (2016) proposed a K-Nearest Neighbor (KNN) approach for measuring bathymetry over a clear coral reef area with large patches of sand and a 20-m depth range. The KNN method resulted in water depths with 0.8 m RMSE using Worldiew-2 satellite images, which outperform the results obtained from Lyzenga linear method. However, a large number of field points, approximately 300,000 points, were required for the training of the algorithm. Gholamalifard et al., (2013) argued that a NN approach was greater than that of PCA for a linear red band correlation using Landsat-5 imagery over a deep water area. This study produced a RMSE of 2.14 m at a depth range of 45 m. Corucci et al., (2011) developed a neuro-fuzzy approach that could be used for bathymetry measurements over a sandy coastal area with clear water using Quickbird images. An RMSE value of about 0.64 m was obtained over a depth range of 14 m with small number of training samples. Our results are comparable to the results obtained from these studies for both the processed images and the NN approach within the same ranges of depths.

Acknowledgement

This research was partly supported by JSPS Gran-in-Aid for Scientific Research (No. 15H02268) and Science and Technology Research Partnership for Sustainable Development (SATREPS) Program, Japan Science and Technology Agency (JST), and Japan International Cooperation Agency (JICA).

6. Conclusions

This article proposed RFE as a hybrid-based approach that could be used for bathymetry measurements. This approach was applied in two different areas that had a different number of available field points: one was a low-turbidity, deep, silt–sand bottomed area of the port of Alexandria, Egypt, with a depth of up to 10.5 m, and the other was a low-turbidity coral reef area of Shiraho Island, Japan, which had a water depth range of 12.5 m. For both NN and SVR methods, the green and red band logarithms that had been corrected for atmospheric and sun-glint systematic errors were set as input data, and the water depths were to be obtained as output data. The proposed RFE approach ensemble the water depths outputs from the NN and SVR approaches. In order to validate the improvements of the produced water depths accuracy from the proposed RFE approach they were compared to the single NN and SVR results. We also compared these results with those of echosounder water depth field data.

The SVR approach yielded RMSE values of 0.96 and 1.03 m over the two study areas, while the NN approach yielded values of 0.84 and 0.98 m. Moreover, the proposed RFE approach produced RMSE values of 0.64 and 0.90 m over the two study areas. From these results, it can be concluded that for bathymetry mapping over diverse areas, the RFE ensemble produced more accurate results than the single SVR or NN approaches.

References

Berk, A., Bernstein, L., Anderson, G., Acharya, P., Robertson, D., Chetwynd, J. and Adler-Golden, S., 1998, MODTRAN Cloud and Multiple Scattering Upgrades with Application to AVIRIS. *Remote Sensing of Environment*, Vol. 65(3), 367-375.

Blakey, T., Melesse, A. and Hall, M., 2015, Supervised Classification of Benthic Reflectance in Shallow Subtropical Waters using a Generalized Pixel-Based Classifier across a Time Series. *Remote Sensing*, Vol. 7(5), 5098-5116.

Brando, V. E., Anstee, J. M., Wettle, M., Dekker, A. G., Phinn, S. R. and Roelfsema, C., 2009, A Physics Based Retrieval and Quality Assessment of Bathymetry from Suboptimal Hyperspectral Data. *Remote Sensing of Environment*, Vol. 113(4), 755-770.

Breiman, L., 2001, Random Forests. *Journal of Machine Learning*, Vol. 45(1), 5-32.

Breiman, L., 2014, Manual on Setting Up, Using, And Understanding Random Forest V3.1. Available from: https://www.stat.berkeley-.edu/~breiman/Using_random_forests_V3.1.pdf. (May 1, 2016).

Ceyhun, Ö. and Yalçın, A., 2010, Remote Sensing of Water Depths in Shallow Waters via Artificial Neural Networks. *Estuarine, Coastal and Shelf Science*, Vol. 89(1), 89-96.

Chust, G., Grande, M., Galparsoro, I., Uriarte, A. and Borja, A., 2010, Capabilities of the Bathymetric Hawk Eye LiDAR for Coastal Habitat Mapping: A Case Study within a Basque Estuary. *Estuarine, Coastal and Shelf Science*, Vol. 89(3), 200-213.

Collin, A., Nadaoka, K. and Nakamura, T., 2014, Mapping VHR Water Depth, Seabed and Land Cover Using Google Earth Data. *ISPRS International Journal of Geo-Information*, Vol. 3, 1157-1179.

Corucci, L., Masini, A. and Cococcioni, M., 2011, Approaching Bathymetry Estimation from High Resolution Multispectral Satellite Images using a

Neuro-Fuzzy Technique. *Journal of Applied Remote Sensing*, Vol. 5(1), 1-15.

Doxani, G., Papadopoulou, M., Lafazani, P., Pikridas, C. and Tsakiri-Strati, M., 2012, Shallow-Water Bathymetry over Variable Bottom Types Using Multispectral Worldview-2 Image. International Archives of the Photogrammetry, *Remote Sensing and Spatial Information Sciences*, Vol. 39(B8), 159-164.

Fuxing, D. and Qian, D., 2003, A Technique for Extracting Water Depth Information from Multispectral Scanner Data in the South China Sea. *Marine Science Bulleting*, Vol. 22(3), 55-60.

Gao, J., 2009, Bathymetric Mapping by Means of Remote Sensing: Methods, Accuracy and Limitations. *Progress in Physical Geography*, Vol. 33(1), 103-116.

Ghimire, B., Rogan, J., Rodriguez-Galiano, V., Panday, P. and Neeti, N., 2012, An Evaluation of Bagging, Boosting and Random Forests for Land-Cover Classiication in Cape Cod, Massachusetts, USA. *GIScience & Remote Sensing*, Vol. 5(5), 623-643.

Gholamalifard, M., Kutser, T., Esmaili-Sari, A., Abkar, A. and Naimi, B., 2013, Remotely Sensed Empirical Modeling of Bathymetry in the Southeastern Caspian Sea. *Remote Sensing*, Vol. 5(6), 2746-2762.

Guan, H., Yu, J., Li, J. and Luo, L., 2012, Random Forests-Based Feature Selection for Land-Use Classification using Lidar Data and Orthoimagery. *XXII ISPRS Congress*, XXXIX: 203-208.

Hedley, J., Harborne, A. and Mumby, P., 2005, Technical Note: Simple and Robust Removal of Sun Glint for Mapping Shallow-water Benthos. *International Journal of Remote Sensing*, Vol. 26(10), 2107-2112.

Heyman, W. D., Ecochard, J. B. and Biasi, F. B., 2007, Low-Cost Bathymetric Mapping for Tropical Marine Conservation—A Focus on Reef Fish Spawning Aggregation Sites. *Marine Geodesy*, Vol. 30, 37-50.

Hoepffner, N. and Zibordi, G., 2009, Remote Sensing of Coastal Waters. In Encyclopedia of Ocean Sciences book (2nd Ed.), 732-741.

Immitzer, M., Atzberger, C. and Koukal, T., 2012, Tree Species Classification with Random Forest Using Very High Spatial Resolution 8-Band WorldView-2 Satellite Data. *Remote Sensing*, Vol. 4, 2661-2693.

Jay, S. and Guillaume, M., 2014, A Novel Maximum Likelihood Based Method for Mapping Depth and Water Quality from Hyperspectral Remote-Sensing Data. *Remote Sensing of Environment*, Vol. 147, 121-132.

Kao, M., Ren, H., Lee, S., Chang, P., Yen, Y. and Lin, H., 2009, Determination of Shallow Water Depth Using Optical Satellite Images. *International Journal of Remote Sensing*, Vol. 30(23), 6241-6260.

Kay, S., Hedley, J. and Lavender, S., 2009, Sun Glint Correction of High and Low Spatial Resolution Images of Aquatic Scenes: A Review of Methods for Visible and Near-Infrared Wavelengths. *Remote Sensing*, Vol. 1(4), 697-730.

Kibele, J. and Shears, T., 2016, Nonparametric Empirical Depth Regression for Bathymetric Mapping in Coastal Waters. *IEEE Journal of Selected Topics in Applied Earth Observations and Remote Sensing*, Vol. 9(11), 5130-5138.

Kim, H. and Sohn, G., 2011, Random Forests Based Multiple Classifier System for Power-Line Scene Classification. *International Archives of the Photogrammetry*, XXXVIII: 29-31.

Landsat-8. 2013, Using the USGS Landsat 8 Product. Available from: http://landsat.usgs.gov/Landsat8_Using_Product.php (January 20, 2016).

Lee, K., Kim, A., Olsen, R. and Kruse, F., 2011, Determination of Bottom-Type and Bathymetry Using WorldView-2. *Proc. SPIE Ocean Sensing and Monitoring III*, 8030.

Lesser, M. and Mobley, C., 2007, Bathymetry, Water Optical Properties, and Benthic Classification of Coral Reefs Using Hyperspectral Remote Sensing Imagery. *Coral Reefs*, Vol. 26(4), 819-829.

Leu, L. and Chang, H., 2005, Remotely Sensing in Detecting the Water Depths and Bed Load of Shallow Waters and Their Changes. *Ocean Engineering*, Vol. 32(10), 1174-1198.

Liu, Z. and Zhou, Y., 2011, Direct Inversion of Shallow-Water Bathymetry from EO-1 Hyperspectral Remote Sensing Data. *Chinese Optics Letters*, Vol. 9(6), 60102-60105.

Louchard, E., Reid, R., Stephens, F., Davis, C., Leathers, R. and Downes, T., 2003, Optical Remote Sensing of Benthic Habitats and Bathymetry in Coastal Environments at Lee Stocking Island, Bahamas: A Comparative Spectral Classification Approach. *Limnology and Oceanography*, Vol. 48, 511-521.

Lyons, M., Phinn, S. and Roelfsema, C., 2011, Integrating Quickbird Multi-Spectral Satellite and Field Data: Mapping Bathymetry, Seagrass Cover, Seagrass Species and Change in Moreton Bay, Australia in 2004 and 2007. *Remote Sensing*, Vol. 3(12), 42-64.

Lyzenga, D. R., 1985, Shallow-Water Bathymetry using Combined Lidar and Passive Multispectral Scanner Data. *International Journal of Remote Sensing*, Vol. 6(1), 115-125.

Lyzenga, D. R., Malinas, N. P. and Tanis, F. J., 2006, Multispectral Bathymetry using a Simple Physically Based Algorithm. *IEEE Transactions on Geoscience and Remote Sensing*, Vol. 44(8), 2251-2259.

Mohamed, H., Abdelazim N., Salah, M., Nadaoka, K. and Zahran, M., 2017, Assessment of Proposed Approaches for Bathymetry Calculations Using Multispectral Satellite Images in Shallow Coastal/Lake Areas: A Comparison of Five Models. *Arabian Journal of Geosciences*, Vol. 10(42), 1-17.

Monteys, X., Harris, P., Caloca, S. and Cahalane, C., 2015, Spatial Prediction of Coastal Bathymetry Based on Multispectral Satellite Imagery and Multibeam Data. *Remote Sensing*, Vol. 7(10), 13782-13806.

Moses, S., Janaki, L., Joseph, S., Gomathi, J. and Joseph, J., 2013, Lake Bathymetry from Indian Remote Sensing (P6-LISS III) Satellite Imagery using Artificial Neural Network Model. Lakes & Reservoirs: *Research & Management*, Vol. 18(2), 145-153.

Pacheco, A., Horta, J., Loureiro, C. and Ferreira, O., 2015, Retrieval of Nearshore Bathymetry from Landsat 8 Images: A Tool for Coastal Monitoring in Shallow Waters. *Remote Sensing of Environment*, Vol. 159, 102-116.

Paringit, E. and Nadaoka, K., 2012, Simultaneous Estimation of Benthic Fractional Cover and Shallow Water Bathymetry in Coral Reef Areas From High-Resolution Satellite Images. *International Journal of Remote Sensing*, Vol. 33(10), 3026-3047.

Paul, C. and Roehl, E. A., 2006, Estimating Water Depths Using Artificial Neural Networks. *In 7th International Conference on Hydro informatics HIC*. Nice, France. 1-8

Piotrowski, C. and Dugan, P., 2002, Accuracy of Bathymetry and Current Retrievals from Airborne Optical Time-Series Imaging of Shoaling Waves. *IEEE Transactions on Geoscience and Remote Sensing*, Vol. 40(12), 2606-2618.

Ranganathan, A., 2004, The Levenberg-Marquardt Algorithm. *Internet httpexcelsior cs ucsb educoursescs*, Vol. 142, 1-5.

Razavi, B., 2014, Predicting the Trend of Land Use Changes Using Artificial Neural Network and Markov Chain Model (Case Study: Kermanshah City). *Research Journal of Environmental and Earth*, Vol. 6(4), 215-226.

Rumelhart, D. E., Hinton, G. E. and Williams, R. J., 1986, Learning Internal Representations by Error Propagation. *In Parallel Distributed Processing: Explorations in the Microstructure of Cognition*. PDP Research Group. Cambridge, MA, USA: MIT Press. (1st Ed.): 318-362.

Sánchez-Carnero, N., Ojeda-Zujar, J., Rodríguez-Pérez, D. and Marquez-Perez, J., 2014, Assessment of Different Models for Bathymetry Calculation using SPOT Multispectral Images in a High-Turbidity Area: The Mouth of the Guadiana Estuary. *International Journal of Remote Sensing*, Vol. 35(2), 493-514.

Smola, A. and Schölkopf, B., 2004, A Tutorial on Support Vector Regression. *Statistics and Computing*, Vol. 14, 199-222.

Stumpf, R., Holderied, K. and Sinclair, M., 2003, Determination of Water Depth with High-Resolution Satellite Imagery over Variable Bottom Types. *Limonology and Oceanography*, Vol. 48, 547-556.

Su, H., Liu, H. and Heyman, W., 2008, Automated Derivation of Bathymetric Information from Multi-Spectral Satellite Imagery using a Non-Linear Inversion Model. *Marine Geodesy*, Vol. 31, 281-298.

Vahtmäe, E. and Kutser, T., 2016, Airborne Mapping of Shallow Water Bathymetry in the Optically Complex Waters of the Baltic Sea. *Journal of Applied Remote Sensing*, Vol. 10(2), 1-16.

Vapnik, V. and Chervonenkis, A., 1964, A Note on One Class of Perceptrons. *Automation and Remote Control*, 25.

Vinayaraj, P., Raghavan, V. and Masumoto, S., 2016, Satellite Derived Bathymetry using Adaptive-Geographically Weighted Regression Model. *Marine Geodesy*, Vol. 39(6), 458-478.

Wahidin, N., Siregar, V., Nababan, B., Jaya, I. and Wouthuyzen, S., 2015, Object-based Image Analysis for Coral Reef Benthic Habitat Mapping with Several Classification Algorithms. *Procedia Environmental Sciences*, Vol. 24, 222-227.

Were, K., Bui, D., Dick, O. and Singh, B., 2015, A Comparative Assessment of Support Vector Regression, Artificial Neural Networks, And Random Forests for Predicting and Mapping Soil Organic Carbon Stocks Across an Afromontane Landscape. *Ecological Indicators*, Vol. 52, 394-403.

Williams, G., 2011, *Data Mining with Rattle and R. The Art of Excavating Data for Knowledge Discovery*. Springer-Verlag New York, book, 293-304.